Proceedings of the ASME 2018 International Design Engineering Technical Conferences & Computers and Information in Engineering Conference
IDETC/CIE 2018
August 26-29, 2018, Montreal, Quebec, Canada

DETC2018/85975

TRAJECTORY PLANNING FOR CONFORMAL 3D PRINTING USING NON-PLANAR LAYERS

Aniruddha V. Shembekar
Center for Advanced Manufacturing
University of Southern California
Los Angeles, California 90089-1453
Email: shembeka@usc.edu

Yeo Jung Yoon
Center for Advanced Manufacturing
University of Southern California
Los Angeles, California 90089-1453
Email address: yeojungy@usc.edu

Alec Kanyuck
Center for Advanced Manufacturing
University of Southern California
Los Angeles, California 90089-1453
Email address: kanyuck@usc.edu

Satyandra K. Gupta
Center for Advanced Manufacturing
University of Southern California
Los Angeles, California 90089-1453
Email: skgupta@usc.edu

ABSTRACT

Additive manufacturing (AM) technologies have been widely used to fabricate 3D objects quickly and cost-effectively. However, building parts consisting of complex geometries with multiple curvatures can be a challenging process for the traditional AM system whose capability is restricted to planar-layered printing. Using 6-DOF industrial robots for AM overcomes this limitation by allowing materials to deposit on non-planar surfaces with desired tool orientation. In this paper, we present collision-free trajectory planning for printing using non-planar deposition. Trajectory parameters subject to surface curvature are properly controlled to avoid any collision with printing surface. We have implemented our approach by using a 6-DOF robot arm. The complex 3D structures with various curvatures were successfully fabricated, while avoiding any failures in joint movement, holding comparable build time and completing with a satisfactory surface finish.

1 Introduction

Several popular additive manufacturing (AM) methods are based on computer controlled material deposition on a planar surface [1–3]. The use of planar layers simplifies the hardware needed to carry out 3D printing. Independent X and Y drives are used to move the deposition head in the horizontal plane to create a layer. The Z drive is used to move the deposition head up and down to create new layers. Each axis can be moved independently and error compensation methods can be developed for each axis. Cartesian configuration used in traditional 3D printing machines enables high stiffness. Even low cost 3D printing machines provide good accuracy and simplify the planning process.

Constructing a part using only planar horizontal layers limits the capabilities of the additive manufacturing processes based on material deposition. Performing material deposition using 6-DOF articulated robot arms can significantly expand the capabilities of the additive manufacturing processes by allowing material deposition on complex non-planar layers. The following three examples illustrate the benefits of using non-planar layers:

1. *Additive manufacturing using composites:* Many composite parts have thin three-dimensional shell structures because of weight constraints. Achieving the right fiber orientation is critical to the proper functioning of these parts. Printing them using the conventional planar-layer material deposi-

tion process orients fibers in the plane of the layer. This often leads to undesirable fiber orientation. Printing such parts will require the ability to position the fibers along a 3 dimensional curve. The capability to deposit the material along non-planar layers is needed to meet this requirement. We envision that a sacrificial scaffold can be created and composite layers can be deposited on top of the scaffold to create parts with the desired fiber orientation and functionality.

2. *Reducing Overall fabrication time in printing of large parts:* Many part geometries require the use of a certain build direction to minimize the staircase effect in a conventional planar layer based process. This in turn may lead to the printing of a large number of layers and can be a very time consuming process. Non-planar layers present more options for minimizing the staircase effect. There are several different types of geometries that can be printed much faster using non-planar layers while minimizing staircase effects on the curved surfaces. Time savings can be significant in the case of large parts by (1) lowering the build time and (2) reducing the need for post processing by minimizing the staircase effect.
3. *Repair of complex parts:* Repairing complex parts requires depositing material on non-planar surfaces and then shaping the deposited material. Robotic 3D printing may enable near-net deposition. The same robot that is used for material deposition can also be used for grinding and sanding. This can significantly simplify the overall process. Being able to deposit material on curved surfaces will enable a higher level of automation in the repair of complex parts. The use of robots in material deposition can also enable in-situ additive manufacturing on prefabricated structures.

The extruded filament from the nozzle is rotationally symmetric along its axis and hence only five degrees of freedom are needed to position and orient the deposition head on a point on a surface. However, to avoid collision of the deposition head with the surrounding features of the surface requires additional degrees of freedom. 6-DOF arms will enable us to perform deposition on complex surfaces.

As discussed earlier, material deposition using a 6-DOF robot arm can significantly expand the capabilities of additive manufacturing. However, this requires addressing several challenges. Planning collision free trajectories along complex curved surfaces for 6-DOF robots is a computationally challenging problem. Performing deposition along curved surfaces requires adjustment of process parameters continuously to ensure that defect-free parts can be produced. This requires constructing a model that relates process parameters to deposition performance.

The purpose of our research is to generate a feasible trajectory for conformal printing by using non-planar material deposition. Trajectory planning includes path and hatching pattern generation, tool orientation calculation and trajectory parameter control to ensure collision-free printing along a curved structure. Feasibility of planned trajectory is validated by using robotic simulation. We implemented the proposed trajectory planning on the robotic AM system which was already built from the previous work done in our group [4]. The system consists of 6-DOF robot arm manipulator, ABB IRB 120, and a custom designed fused deposition modeling (FDM) extruder.

2 Related Work

Use of industrial robots for additive manufacturing has recently gained interest in both academia and industry [5–8]. 6-DOF robot arms make it possible to fabricate 3D parts at various angles, which overcomes the limitations of conventional 3D printing methods. Zhang et al. [5] presented a marketing survey on potential use of robotic additive manufacturing and feasibility study of its applications. The paper addressed robotic direct metal deposition as an ideal alternative to high precision CNC machines because of its accuracy demand, flexibility and larger reachability compared to these CNC machines. Brooks et al. [6] presented the design, development and testing of a robot-assisted printing system of biopolymer thin shells. The FDM system directly deposited pellets of biomaterial onto 3D curved surfaces supported by a 6-DOF robot arm. Keating et al. [7] developed a robotic system supporting multi-functional and multi-material processes including additive, formative and subtractive fabrication. The main focus in this paper was developing a uniform platform capable of performing the above three functional processes. There was additional research on developing a low-cost 3D printer using a Stewart mechanism, which mainly consists of six linear actuators, by Song et al. [9]. In their system, a laser-camera is used to correct backlash errors so materials can be accurately deposited on surfaces, while eliminating the risk of collision. Trajectory planning for additive manufacturing system has been studied to improve printing speed, save materials, and reduce energy use of the system [10–12]. Sheng et al. [10] presented a decomposition-based approach which models a surface partitioning problem in the geometric domain. Ganganath et. al [11] modified conventional traveling salesman problem and adapted it to a trajectory planning for 3D printing to obtain time-efficient trajectories.

When using a robot in 3D printing, more parameters are to be considered for trajectory planning because the system is subject to task space constraints. If a robot encounters a collision or joint limit along the planned trajectory, the trajectory is invalid and the system should regenerate a feasible trajectory. Altering material deposition directions, generating different hatching patterns, decreasing joint angle velocities or repositioning the initial configuration of the robot can all be possible solutions to finding a viable trajectory. There have been extensive amounts of

research on trajectory planning and optimization for use on industrial robots in various tasks such as welding [13, 14], painting [15, 16], cleaning [17] and finishing [18]. For robotic additive manufacturing processes, Ding et al. [19] introduced adaptive path planning for wire-feed AM by using medial axis transformation. The proposed algorithm was implemented by robotic wire and arc AM system and resulted in material savings, void-free deposition, and improved accuracy at the boundary. This research presented the enhanced additive manufacturing algorithm, however, minimal work was done on robotic trajectory planning which will be covered in our work. Another research project was done on a robotic AM process along the direction of curved surfaces by Zhang et al [20]. In the author's other work [21], robotic AM process is simulated by using the software RobotStudio and the fabrication process is performed. However, the printing resulted in curled fiber in the build and showed differences compared to the simulation. In our work, we selected appropriate input parameters to achieve desired surface finish and were able to successfully fabricate the 3D object with complex surfaces.

The main focus of the previous work done in our group [4] was on the hardware system development, printing process planning, and mechanical testing and analysis of produced parts in different loading configurations. In our paper, we emphasize the trajectory planning for non-planar layered printing and its feasibility; the trajectory is generated using a point projection method as opposed to a slicing one, and process parameters are generated from simulations and empirical experiments. After the feasibility of the trajectory is verified by robotic simulation, the printing process is performed.

3 Trajectory Planning

3.1 Overview

Following are two general approaches to solve trajectory planning problem of 6-DOF robot arm moving along a curve in 3D Cartesian coordinates.

1. *Solving inverse kinematics(IK) and performing graph-based search*: In semi-constrained Cartesian trajectories in 3-D space, the set of sample points $\mathcal{S} = \{p_i : i = 1,2,\ldots,n\}$ along the trajectory can be selected. Let $P_i = (x_i, y_i, z_i, R_{x_i}, R_{y_i}, R_{z_i}) \in \mathbb{R}^6$ be the corresponding positions and orientations of the end effector at each sample point p_i. We can solve inverse kinematic equations to find a set of possible joint values of the robot arm at a given P_i, $Q_i = (q_{1_i}, q_{2_i}, q_{3_i}, q_{4_i}, q_{5_i}, q_{6_i})$. For one given configuration of the robot arm, there can be multiple joint solutions [22]. The next step is to design a structure of a graph model for the viable joint solutions and perform a graph-based search by connecting nodes in time. A node corresponds to a solution, so if we can find a connection between the previous node and the current node, $[Q_{i-1} \rightarrow Q_i]$ we know that the robot can shift the from previous joint solution to the current solution without collision or singularity. So, the continuous connection between the nodes $[Q_{i-1} \rightarrow Q_i]$ in the proposed graph model implies an existence of a feasible trajectory $[P_{i-1} \rightarrow P_i]$. When all possible connections of the nodes are explored, we can choose the one with the shortest trajectory or the one with minimal joint movement.
2. *Solving inverse Jacobian and integrating over the domain*: Using the same notation as shown in approach 1, the set of sample points along the trajectory can be selected. For the given position and orientation of the end effector P_i, the velocity can be denoted as $\dot{P}_i = (\dot{x}_i, \dot{y}_i, \dot{z}_i, \dot{R}_{x_i}, \dot{R}_{y_i}, \dot{R}_{z_i}) \in \mathbb{R}^6$ where the first three values indicate velocity of the end effector and the last three values represent the angular velocity of the end effector. The possible joint velocity of the robot arm at a given $\dot{P}_i$ will be $\dot{Q}_i = (\dot{q_{1_i}}, \dot{q_{2_i}}, \dot{q_{3_i}}, \dot{q_{4_i}}, \dot{q_{5_i}}, \dot{q_{6_i}})$ To avoid IK calculations, the problem is formulated in velocity space $\dot{P}_i = J(q)\dot{Q}_i$, where inverse Jacobian for each point is calculated $\dot{Q}_i = J^{-1}(q)\dot{P}_i$. Then by integration, the joint values at the next point Q_2 can be obtained. By using the sequential method, we can obtain joint values of all sample points and generate the trajectory.

To generate the trajectory for our robotic system, we have used an in-built IK solver from the RobotStudio program offered by ABB. The program internally computes the best possible robot configuration for a given point and create a trajectory from given input parameters related to position and orientation. Hence, our main focus is to find the appropriate set of input parameters generate a path in order to allow material to be accurately deposited at a desired position, direction and velocity. We assigned input parameters and simulated a robot's movement in RobotStudio. If there is any singularity along the trajectory, position that is out of reachability, or trajectory that is not feasible for the control system, RobotStudio automatically outputs errors. In this case, we modified the input parameters and performed another simulation.

3.2 Path generation on non-planar layer

The main idea behind generating a path is to create the sequences of position and orientation of the tool center point (TCP) to form hatching lines covering the entire surface. STL files of non-planar surfaces include the set of unit normal vectors and information on vertices of each triangle in 3D Cartesian coordinates. By projecting this data on 2D Cartesian coordinate plane, we can obtain the shape of the projected surface. Then we can create a uniformly spaced zigzag path within the projected surface where spacing matches the thickness of the filament to be extruded. Finally, the zig-zag path is projected back to the printing surface, which creates the path in 3D Cartesian coordinates.

Orientation of the FDM extruder corresponding to the position of the extruder is also calculated. The default setting for extruder orientation can be normal to the surface but there is a

risk that the extruder tip or heating block may hit the mold while printing on a concave surface. To account for this, we multiply an adjustment factor α to the default printing angle. This prevents the extruder from collision and creates a smooth surface finish as the change in joint angles is reduced. The value of α is gained empirically; several values were tested and the one that generated the best print quality, in terms of smoothness along the curvature, was selected. This empirical value ranges from 0.25 to 0.75. The orientation about the Z-axis is equal to zero because the extruder tip is symmetrical along the Z-axis.

The path generation process is mostly performed by MATLAB software. Input data is of STL file format, containing the shape information of the object to print, and the final output data is generated in the form of RAPID data to be used in RobotStudio.

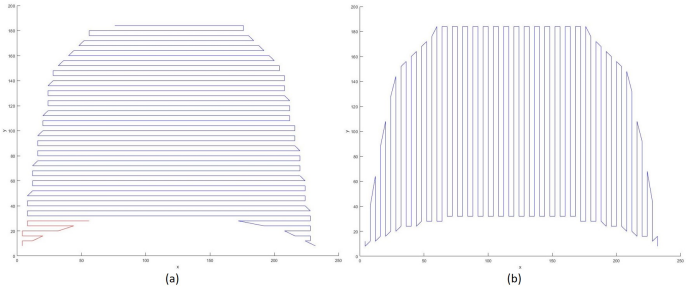

Figure 1. (a) Hatching along X-axis, (b) Hatching along Y-axis

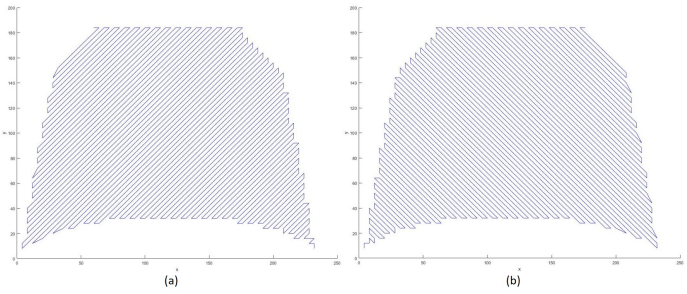

Figure 2. (a) Hatching along 45^o slope, (b) Hatching along 135^o slope

3.3 Selection of hatching direction

When printing layer by layer, users can choose a hatching pattern among various options such as: zigzag, contour or spiral, as well as the hatching direction. In most of cases, we designed hatching direction to be a 90^o difference over layers; for a zigzag hatching, if the first layer is printed along the X-axis (0^o slope), the consecutive layer will be printed along the Y-axis (90^o slope) and the layer after that will be printed again along the X-axis as shown in Figure 1. Another factor considered was path continuity, whether hatching is continuous over a layer. For example, in Figure 1, printing along the Y-axis is continuous over the surface but not when printing along the X-axis, which leaves the red lines in the figure to be printed separately. On the other hand, hatching along 45^o for one layer and 135^o slope for next layer ensures path continuity as shown in Figure 2. In such case, printing along 45^o & 135^o slope was selected over printing along 0^o & 90^o slope.

3.4 Algorithm

To create a trajectory on a non-planar surface, we use a projection method instead of a slicing algorithm which transforms 3D objects to individual layers. From the STL file, information about vertices, faces and unit normal vectors of triangles is obtained and stored in arrays [v], [f] and [n] respectively. Based on the maximum value of x and y coordinates in [v], grid points data P_{grid} is generated over the XY plane. The grid spacing is 0.5mm for the presented work and this size is determined based on the measured thickness of deposited materials, which is around 0.48-0.52mm. It is treated as an input and can be changed depending upon the complexity of curvature in the given part. From all normals [n], only normals with negative co-efficient of $\hat{k}$ are stored separately as $[n_{bottom}]$. The vertices associated with $[n_{bottom}]$ are projected on the XY plane, projecting 3D triangle to the XY plane. Each projected triangle stores the grid points which lie inside the triangle, P_{in}. These grid points are projected back on the original 3D triangle by storing in $P_{in,projected}$. Since any plane needs the minimum of three points to define the plane equation, vertices of the triangle generate the equation of the plane and the corresponding z-coordinate value for all grid points inside the triangle is obtained. The process is repeated for all triangles and the uniform grid points data is obtained along a conformal surface.

In $P_{in,projected}$, information on unit normals associated with STL triangles is stored. This information is useful in calculating rotation angles for the TCP as $R_x = -tan^{-1}(n_y/n_z)$ & $R_y = tan^{-1}(n_x/n_z)$. After getting projected points, hatching direction is decided by user inputs. Based on the hatching direction, projected points are grouped into parallel hatching lines and every alternate array of a line is flipped to get the zig-zag pattern for printing. This process is repeated for each layer. Algorithm 1 presents hatching along 0^o slope for the first layer and 90^o slope for the consecutive layer.

4 Trajectory parameters

Print speed, extent of spline motion (zone data in RobotStudio) and acceleration/deceleration inputs are three main process parameters which need to be adjusted before printing. Print speed, consisting of proportionate TCP speed, joint angle veloc-

Algorithm 1 Path Generation from STL File

START
Input STL file, hatching space and gap between layers
PathType ← hatching direction
$v \leftarrow$ vertices from STL file // $v : [x, y, z]$
$f \leftarrow$ faces from STL file // $f : [v_i, v_j, v_k]$
$n \leftarrow$ unit normal value from STL file // $n : [n_x, n_y, n_z]$
xmax ← $max(x)$, ymax ← $max(y)$
Create grid points P_{grid} = [0:xmax,0:ymax] //on XY plane
for all i = 1:N **do**
{
if $n_z[i] < 0$ **then**
Store $\{v_{bottom}, f_{bottom}, n_{bottom}\} \leftarrow \{v(i), f(i), n(i)\}$
// identify bottom surface
end if
}
end for
for all i = 1:size(f_{bottom}) **do**
{
Identify v_{bottom} which belongs to $f_{bottom}[i]$ //to get vertices of each triangle
$v_{z\_bottom} \leftarrow 0$ //Project v_{bottom} on XY plane
Find all $P_{in} \in P_{grid}$ inside triangle
for all j = 1:size(P_{in}) **do**
{
Project $P_{in}[j]$ on $f_{bottom}[i]$
$R_x[j] \leftarrow tan^{-1}(n_{y\_bottom}[i]/n_{z\_bottom}[i])$
$R_y[j] \leftarrow tan^{-1}(n_{x\_bottom}[i]/n_{z\_bottom}[i])$
Store $\{P_{in,projected}[j], R_x[j], R_y[j]\}$
}
end for
end for
Case 0 degree PathType
//hatching along x direction
for all i = 1:size($P_{in,projected}$) **do**
group sorted $P_{in,projected[i]}$ along line parallel to x-axis
if i = EVEN **then**
flip $P_{in\_projected[i]}$ //to create zig-zag pattern
end if
end for
Case 90 degree PathType
//hatching along y direction
for all i = 1:size($P_{in,projected}$) **do**
group sorted $P_{in,projected[i]}$ along line parallel to y-axis
if i = EVEN **then**
flip $P_{in,projected[i]}$ //to create zig-zag pattern
end if
end for
END

ity, and extrusion rate indicates how fast a nozzle moves and how fast material is deposited while printing. The print speed and the material deposition rate have significant impacts on printing quality and the strength of a 3D printed object. In traditional additive manufacturing, the slower speed usually results in better quality. Also, print speed can be consistent over a planar surface, keeping the quality level the same. However, in non-planar printing where material is deposited at various angles, uniform speed does not guarantee the same print quality due to the curvatures and complexity of surface. If surfaces have high curvatures and require substantial orientation changes, trajectory parameters should be controlled in order to minimize vibration, to ensure reliability of printing, and to reduce risk of conflicts between a nozzle tip and mold. In order to have variable velocity during motion, accurate velocity control is required as explained in the section 4.1.

Another trajectory parameter to consider is the blending of point to point motion into a spline (zone data), which affects smoothness of a trajectory by creating a few trajectory points as fly-by points when the TCP is traveling along multiple points. This is one of the important criteria in minimizing robot vibrations while printing. Proper value is assigned by an empirical method; several zone data values were tested and the one resulting in the smoothest surface was selected.

The third important criteria in robot movement when traveling form one point to another is acceleration and deceleration. In our work, these values are usually kept below 50% of the maximum to minimize jerks in the system.

4.1 Velocity control

In planar 3D printing, there is no change in rotation angles (R_x, R_y & R_z) of tool since the extruder does not orient about its tool center point. Hence, hatching can be generated with almost constant extruder velocity and extrusion flow rate without affecting the print quality. On the other hand, non-planar 3D printing has active TCP orientation which demands variation in both extruder speed and extrusion flow rate.

When a robot travels along sharp curves, there is a significant change in rotation angles for adjacent points. During this motion, the robot joints should cover large angles while the TCP covers comparatively smaller distance. Figure 3 shows TCP orientation along different surfaces. If the robot joint speeds are constant throughout the motion, the time taken to change joint angles is high which results in more material extrusion along a shorter path. It creates an accumulation of material and distorts subsequent layers over it. This can be prevented by accurately controlling the extrusion flow rate and changing the robot velocity by detecting curvature along every print.

Experiments are performed in order to obtain the maximum extrusion flow rate without creating overflow of material inside the nozzle. Robot velocity is finely tuned relative to extrusion

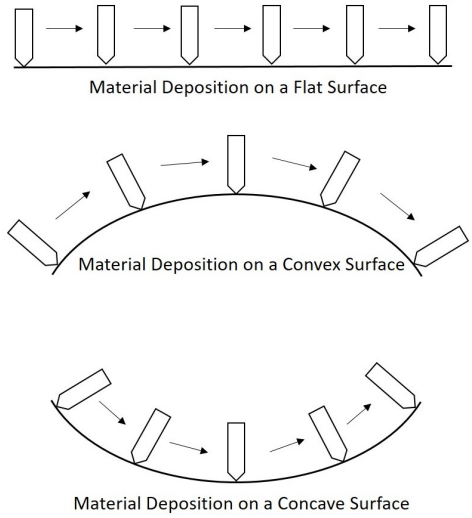

Figure 3. Changes in TCP orientation along a planar, convex and concave surface

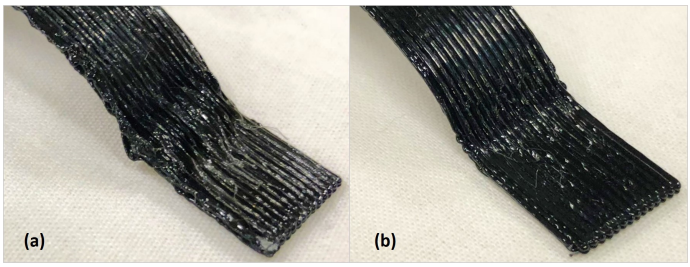

Figure 4. Printing along a curved surface (a) without velocity control, (b) with velocity control

rate to make hatching smooth and uniform. When the robot is moving along a curve, excess material deposition can be reduced either by reducing the material flow or by increasing the robot joint angle speed. Both methods can be applied either independently or together for better material deposition control. While increasing the robot joint speed, there is a possibility that any joint angle may reach speed limit that would stop the entire printing process. Such a scenario can be handled by keeping joint angle speed under the upper limit, reducing the TCP speed and further lowering the extrusion flow rate.

Globally determining the curvature of a printing surface is not always possible. Hence, the nature of the surface is analyzed in a more discretized manner, that is, between two consecutive projected grid points. Since the grid spacing is an input variable, even small curvatures can be identified by resizing the grid mesh. For every projected point and its associated normal, another temporary point is generated along the normal at specific distance from the original point. This distance tends to vary from 1 to 4mm and it can be empirically decided based on experimentation. The gap between consecutive temporary projected points is then compared with original projected points. If the gap between temporary points is more than that of the actual gap then curvature is convex, and vice versa. In any of the cases, robot joint angles vary due to curvature. Hence material extrusion rate is reduced by same amount as that of the gap between temporary projected points and actual projected points. For general estimation of flow rate, linear interpolation can be applied between extreme values (upper and lower limit) of gap and motor micro-stepping delay (maximum and minimum delay possible under specific micro-stepping). This results in precise control over the extrusion rate while constantly changing the slope along the curve. Since extrusion rate by default is kept at maximum, velocity control will only reduce the flow rate along areas of sharp curvature. Extrusion rate can be easily integrated with robot system by generating either analog or digital output signal from the robot controller and sending it to a microcontroller between every motion command to change the stepper motor speed.

A similar approach can be used to control the robot joint angles speed by interpolating it against higher and lower gap values. Unlike flow control, joints speed control can be directly added in motion command by assigning respective joints angle speed to each motion. As joint speed increases along the curve from its initial value, there is a possibility that the joints angular speed reaches its limit. This can be eliminated by identifying the joint angle speed limit in RobotStudio simulation and keeping the highest value of joint angle velocity along the path just below this limit. The highest velocity value is mapped by calculating scale down factor and all remaining velocities are decreased to match the scale. This scale is used to reduce extrusion rate further in order to maintain the uniform layer.

Figure 4 shows the comparison between non-planar printing with and without velocity control for the curved structure. Absence of velocity control deposits extra material on the fillet as shown in Figure 4 (a). On the other hand, Figure 4 (b) shows smoother hatching at fillet with velocity control.

5 Robot Calibration

During the printing process, the gap between the hot nozzle tip of the FDM extruder and the previous layer (or workpiece in the case of the first layer) should be accurate and uniform across the complete conformal surface. Even the slightest variation in gap adversely affects the smoothness of layers, which further affects consecutive layers. In extreme conditions, significant amount of variation in gap increases the risk that end extruder will hit the base and result in a print failure. Figure 5 shows the damaged base and broken build due to improper calibration. This failure incident damages both the end extruder and the base for printing. Additionally, it increases the chance of motor failure in the robotic manipulator due to excess load. To avoid this, the precise calibration of the nozzle tip with respect to the

printing base is required.

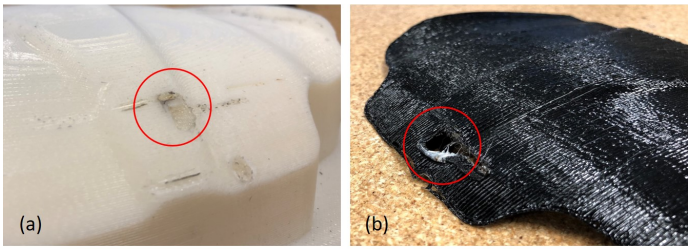

Figure 5. (a) Damaged base, (b) printed model of scaled down version of car bonnet

While calibrating, the following two important factors should be taken into consideration;

1. *Proper offset value of nozzle tip from surface*: The offset between the end of the nozzle tip and the printing surface should match the desired layer thickness to print. If the gap is smaller than the proper value, thickening of hatching lines takes place as extra material between gaps is squeezed out from side. This extra material creates a hindrance to consecutive hatching lines and distorts their path [Figure 6 (a)]. On the other hand, if the gap is greater than the desired value, the layer starts to curl up and will fail the print [Figure 6 (b)].

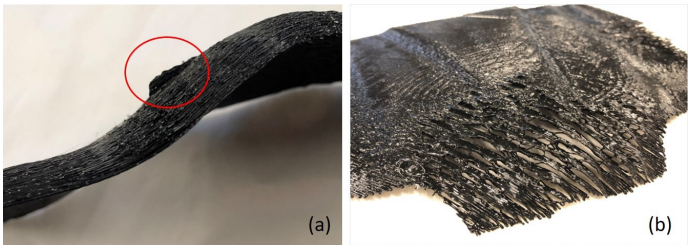

Figure 6. (a) Squeezed out excess material, (b) Curling of hatch pattern

2. *Uniform TCP orientation over the entire space*: If the robot's tool data is poorly calibrated, TCP shifts its position (x, y, z) up to a certain extent when rotated about axes. This creates an uneven thickness in layers. Even though the change in position co-ordinates is very small, the difference is noticeable because the layer thickness is as small as 0.4 mm.

Due to varying constraints involved in initial setup such as small deviation in 3D printed mold base from its actual CAD model or extruder tip wear, calibration is performed every time a new base is mounted. The steps of the calibration process are as follows:

1. *Calculation of accurate tool data & load data*: To get highly accurate data of the TCP for uniform TCP orientation, tool data is calculated with at least seven data points in the procedure. Figure 7 shows the Tool Center Point calibration before printing.
2. *Mounting a base to the proper position on table*: Before a base, where the non layer printing will be held, is actually mounted on a flat table, a RobotStudio simulation is performed. This is done by placing the base at an appropriate place to confirm that the robot has neither a singularity nor a collision over the entire region as shown in Figure 8. The appropriate place should be within the workspace of the robot and should not be too close or too far from the robot since it can increase the chance of reaching joint limits of the robot. The initial position is validated by RobotStudio. If the program has generated errors, then the initial position is re-selected and the selection is done by the user. When confirmed, the base is firmly attached to the table to make sure that it does not get disturbed while printing.

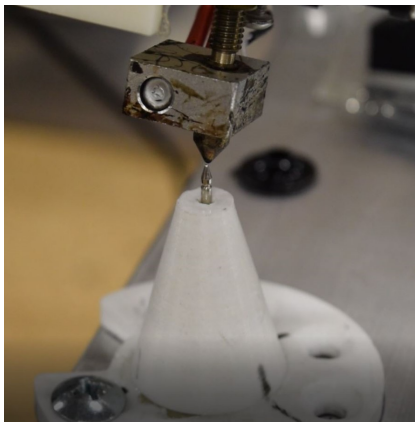

Figure 7. Tool Center Point calibration

3. *Calibration of Z-axis offset value*: At least 3 points along the boundary and 3 points over the surface are selected and TCP is moved to each point with its required rotation about axes. Correct offset is recorded considering the thickness of the desired layer.
4. *Pilot run along boundary of printing surface*: After Z-axis offset, a calibration test is performed along the boundary to ensure that the offset is uniform over the surface and the calibration is reliable.

The complete calibration procedure is followed for every new

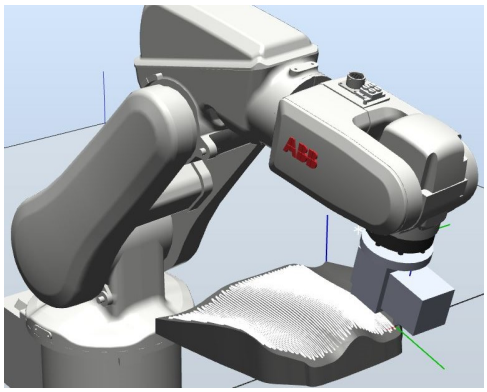

Figure 8. RobotStudio Simulation for singularity and collision check

base mounted in order to avoid damage to any of the hardware used in printing.

6 Printing process

Figure 9 represents the flowchart of printing process we have done with our robotic 3D printing system.

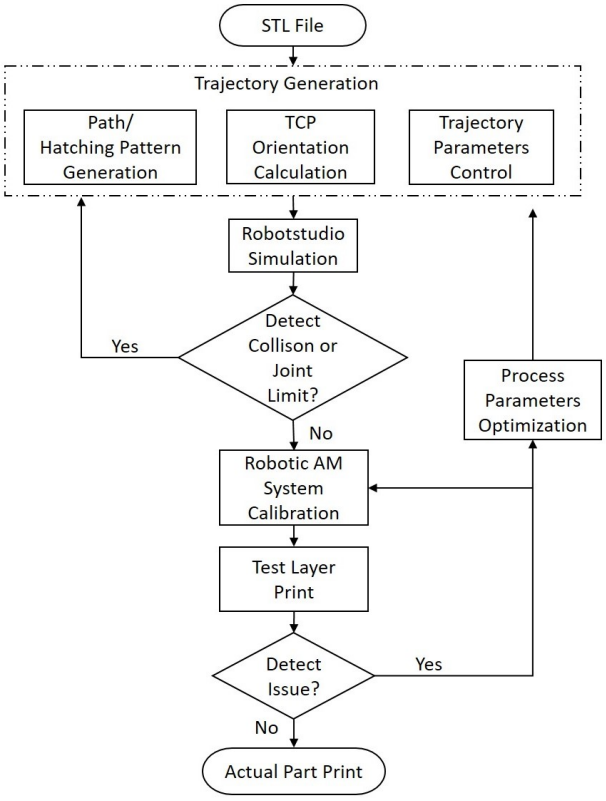

Figure 9. Flowchart of printing process

7 Results

7.1 Path generation on non-planar layer

Using the algorithm discussed in section 3.4, building paths were successfully generated on surfaces with complex geometries. Figure 10 shows the path after the algorithm was implemented in MATLAB. This is a zigzag path that was generated on the non-planar layer by using the projection method. The proposed projection based algorithm is an efficient way to create various hatching patterns along curved surfaces without slicing a 3D object. Users are able to select a number of parameters including hatching pattern/direction, grid size, and surfaces to print.

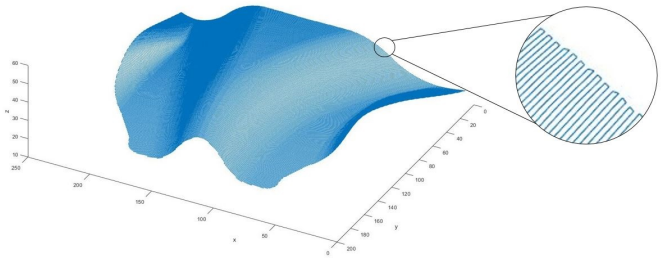

Figure 10. Path generation in MATLAB

7.2 Part Fabrication

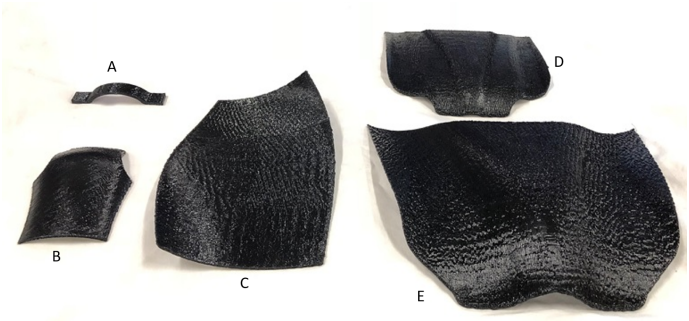

Figure 11. Specimens of different sizes and shapes

Specimens of five different sizes and shapes were fabricated after implementing the trajectory planning algorithm on the robotic additive manufacturing system described in this paper. Figure 11 displays the representative samples of different shapes (Specimen A to Specimen E). The specimens were successfully

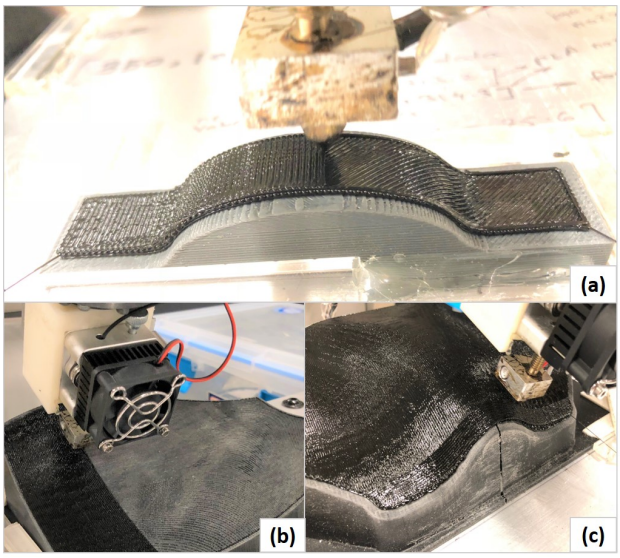

Figure 12. Non-planar 3D Printing of (a) specimen A, (b) specimen C, (c) specimen E

fabricated while using conformal printing along non-planar surfaces. The generated surfaces hold satisfactory texture without gap or excessive filament. Variety in curvature surface and size of the specimens shows the capability and reliability of the proposed algorithm and printing process. Figure 12 shows the printing process of Specimen A, C and E respectively. The material used was PLA filament and the thickness of the deposited filament was 0.5mm. Figure 13 shows the original CAD model design and the corresponding printing results of each specimen. The names, description and nominal sizes of the specimens are shown below:

1. Specimen A : Curved beam (65 x 14 x 4mm)
2. Specimen B : Mini armor chest protector (96 x 70 x 3mm)
3. Specimen C : Wind turbine blade (178 x 127 x 3mm)
4. Specimen D : Mini Car Bonnet 1 (152 x 130 x 2.5mm)
5. Specimen E : Mini Car Bonnet 2 (230 x 178 x 2mm)

Specimen A was fabricated by using a conformal deposition pattern along the length of the beam (0^o). Specimens B,C,D,E were produced by using two conformal deposition patterns (0^o & 90^o), which means the specimens were alternately printed along the length and width. The hatching spacing used for printing is 0.5mm which matches the diameter of the deposited filament.

Comparing the printing result of each specimen, Table 1 shows the thickness, number of layers, weight, measured build time (when using the robotic 3D printing system in this paper), and estimated build time (when using the commercial layer-based FDM 3D printer, Ultimaker 3 Extended). The build time was measured from when the robotic non-planar 3D printing system started working until the work was done. This time does not include time to print support materials. To achieve desired surface finish, several speed values were tested and the one resulting in the best surface smoothness was selected. The build time using the commercial 3D printer was estimated by using Cura software given from a manufacturer. For estimated build time, standard print speed was set to 70mm/s and layer thickness was set to 0.5mm. For fair comparison, the time for printing support materials was also excluded.

Our robotic 3D printing system with non-planar layering showed competitive build time compared to that of the commercial 3D printer with planar-layered method. The build time is governed by the shapes, sizes and number of layers of the part. It is also affected by printing speed to achieve desired printing quality.

7.3 Surface Roughness

Along with build time, surface quality of all five specimen were evaluated using surface roughness measuring instrument Mitutoyo SJ-410. For each specimen, five points were selected randomly and roughness values were measured along the hatching direction. Figure 15 shows location 1 to 5 for each specimen where testing was done. The average roughness value for each specimen was calculated from all locations as shown in Table 2. All average values were around 2 μm or less, which shows the satisfactory performance of non-planar 3D printing process in terms of surface quality.

To evaluate differences in surface finish between non-planar layered prints and planar layered prints, the specimen A_{planar} and C_{planar} were additionally fabricated by using the commercial 3D printer, Ultimaker 3 EXT. Specimen A_{planar} was printed from the same STL file as that of specimen A. Both are the same geometry and size, however notable differences in surface finish were observed. As shown in Figure 14 (a), specimen A_{planar} failed to achieve conformal printing on curved structures by planar deposition. Due to the staircase like shape terminations along the curvature, their surface roughness was not measured. In contrast, specimen A showed a relatively smooth surface without the discrete layer terminations. Similar result were observed in specimen C_{planar}, as shown in Figure14 (b), which has the same wind turbine blade geometry as specimen C. Figure 14 (c) illustrates the differences in surface texture between the non-conformal and conformal specimens. The printing patterns in specimen C_{planar} were neither uniform nor evenly spaced over the surface whereas the pattern in specimen C was evenly spaced with a zigzag pattern. Also, non-conformal specimen show various distinct terminations and fail to achieve satisfactory surface smoothness.

8 Conclusions

This paper presents trajectory planning for conformal additive manufacturing by using non-planar layers. We applied the

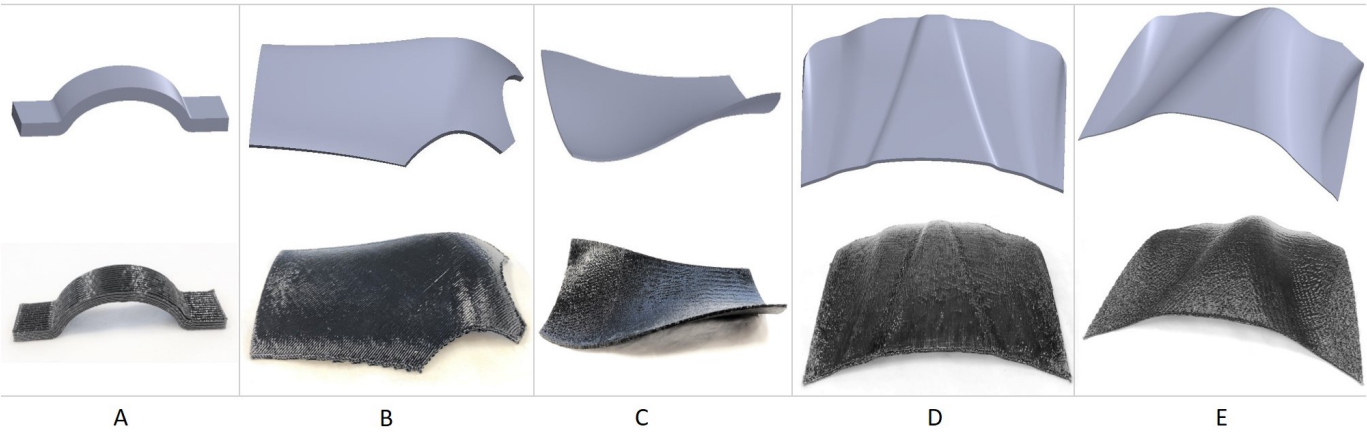

Figure 13. CAD models designed in SolidWorks and actual models printed by the robotic 3D printing system: Specimen A, B, C, D, E from left to right

Specimen	Thickness(mm)	Number of layers	Weight(g)	Measured build time(min), Non-planar	Estimated build time(min), Planar
A	4	8	4.2	14	15
B	3	6	15.4	48	58
C	3	6	57.0	222	217
D	2.5	5	38.3	175	211
E	2	4	49.2	208	226

Table 1. Build Time Comparison between Planar and Non-planar printing

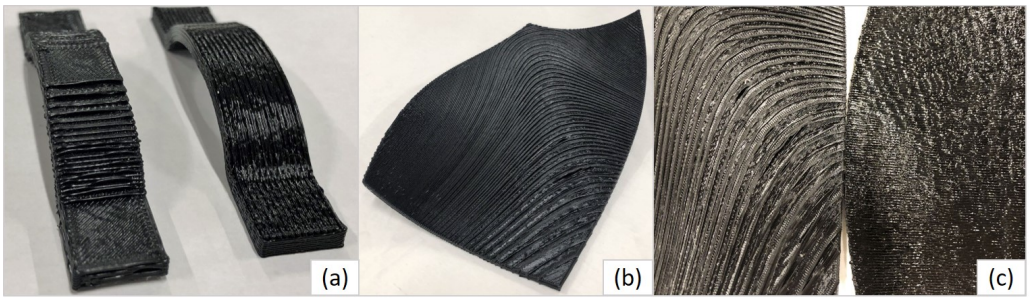

Figure 14. (a)Surface Finish Comparison between Specimen A_{planar}(left) and Specimen A(right), (b) Specimen C_{planar} printed by the traditional 3D printer using planar layered method, (c) Enlarged pictures of Specimen C_{planar}(left) and Specimen C(right)

proposed trajectory algorithm and performed the printing process to the additive manufacturing system with a 6-DOF robot arm. The system was able to successfully fabricate complex parts with multiple curvatures. Results indicated that:

1. A 6-DOF robot arm enables conformal printing on non-planar surfaces. Trajectory planning of printing process should generate appropriate hatching and TCP orientations to ensure a planned trajectory is viable without encountering collisions or joint-limits.
2. Projection based path generation is an effective way of generating various hatching patterns on non-planar surfaces as projecting points along a curvature gives the freedom to generate a path along any direction.
3. Velocity control enables appropriate amount of material to be deposited along sharp curvatures, ensuring that surface

Surface Roughness, R_a (μm)					
Location	Specimen A	Specimen B	Specimen C	Specimen D	Specimen E
1	1.33	0.86	3.49	0.72	2.08
2	1.82	1.97	2.46	1.27	2.13
3	1.47	1.80	1.61	1.10	1.42
4	1.63	1.61	2.40	1.18	0.95
5	0.71	1.61	1.42	1.19	2.41
Mean	1.390	1.574	2.274	1.088	1.798

Table 2. Surface Roughness Values for Specimen A-E at Given Locations

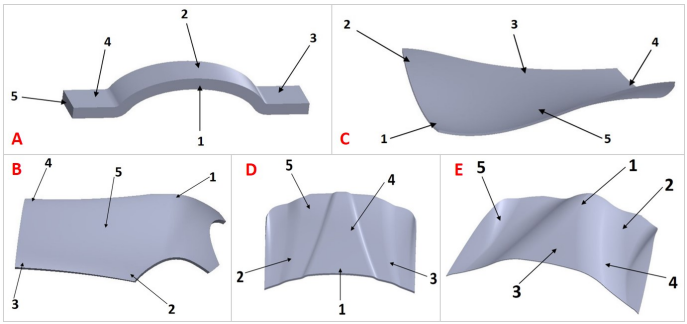

Figure 15. Surface Roughness Measurement Locations 1-5 for Each Specimen A-E

quality is uniform throughout the layer.

4. Specimen built with conformal printing showed comparable build time and a satisfactory surface finish over curvatures, whereas specimen printed with traditional planar layering showed discrete termination on curved surfaces.

In the future, we plan to incorporate automatic selection of hatching pattern and direction based on structural analysis, which will ensure an improved mechanical strength of part. We also plan to perform the conformal 3D printing with two FDM extruders so that support structures can be generated over curvatures and more complex geometries can be fabricated.

9 Acknowledgements

This work is supported in part by National Science Foundation Grants #1634431 and Viterbi Graduate School Merit Fellowship for Yeo Jung Yoon. Opinions expressed are those of the authors and do not necessarily reflect opinions of the sponsors.

REFERENCES

[1] Campbell, I., Bourell, D., and Gibson, I., 2012. "Additive manufacturing: rapid prototyping comes of age". *Rapid Prototyping Journal,* ***18***(4), pp. 255–258.

[2] Gao, W., Zhang, Y., Ramanujan, D., Ramani, K., Chen, Y., Williams, C. B., Wang, C. C., Shin, Y. C., Zhang, S., and Zavattieri, P. D., 2015. "The status, challenges, and future of additive manufacturing in engineering". *Computer-Aided Design,* ***69***, pp. 65–89.

[3] Thompson, M. K., Moroni, G., Vaneker, T., Fadel, G., Campbell, R. I., Gibson, I., Bernard, A., Schulz, J., Graf, P., Ahuja, B., and Martina, F., 2016. "Design for additive manufacturing: Trends, opportunities, considerations, and constraints". *CIRP Annals,* ***65***(2), pp. 737–760.

[4] Abdullah T. Alsharhan, T. C., and Gupta, S. K., 2017. "Enhancing mechanical properties of thin-walled structures using non-planar extrusion based additive manufacturing". In ASME 2017 12th International Manufacturing Science and Engineering Conference collocated with the JSME/ASME 2017 6th International Conference on Materials and Processing, Vol. 2: Additive Manufacturing; Materials, American Society of Mechanical Engineers.

[5] Zhang, G. Q., Li, X., Boca, R., Newkirk, J., Zhang, B., Fuhlbrigge, T. A., Feng, H. K., and Hunt, N. J., 2014. "Use of industrial robots in additive manufacturing - a survey and feasibility study". In ISR/Robotik 2014; 41st International Symposium on Robotics; Proceedings of, VDE, pp. 1–6.

[6] Brooks, B. J., Arif, K. M., Dirven, S., and Potgieter, J., 2017. "Robot-assisted 3d printing of biopolymer thin shells". *The International Journal of Advanced Manufacturing Technology,* ***89***(1), pp. 957–968.

[7] Keating, S., and Oxman, N., 2013. "Compound fabrication: A multi-functional robotic platform for digital design and fabrication". *Robotics and Computer-Integrated Manufacturing,* ***29***(6), pp. 439–448.

[8] Bhatt, P. M., Peralta, M., Bruck, H. A., and Gupta, S. K., 2018. "Robot assisted additive manufacturing of thin multifunctional structures". In ASME 2018 13th International Manufacturing Science and Engineering Conference collocated with the 46th NAMRI/SME North American Manufacturing Research Conference, American Society of Mechanical Engineers.

[9] Song, X., Pan, Y., and Chen, Y., 2015. "Development of a low-cost parallel kinematic machine for multidirectional additive manufacturing". *Journal of Manufacturing Science and Engineering,* ***137***(2).

[10] Sheng, W., Xi, N., Chen, H., Chen, Y., and Song, M., 2003. "Surface partitioning in automated cad-guided tool planning for additive manufacturing". In Proceedings 2003 IEEE/RSJ International Conference on Intelligent Robots and Systems (IROS 2003) (Cat. No.03CH37453), Vol. 2, pp. 2072–2077.

[11] Ganganath, N., Cheng, C. T., Fok, K. Y., and Tse, C. K., 2016. "Trajectory planning for 3d printing: A revisit to traveling salesman problem". In 2016 2nd International Conference on Control, Automation and Robotics (ICCAR), pp. 287–290.

[12] Jin, Y., Du, J., and He, Y., 2017. "Optimization of process planning for reducing material consumption in additive manufacturing". *Journal of Manufacturing Systems,* ***44***, pp. 65–78.

[13] Liguo Huo, L. B., 2008. "The joint-limits and singularity avoidance in robotic welding". *Industrial Robot: the international journal of robotics research and application,* ***35***(5), pp. 456–464.

[14] Wang, X., Shi, Y., Ding, D., and Gu, X., 2016. "Double global optimum genetic algorithmparticle swarm optimization-based welding robot path planning". *Engineering Optimization,* ***48***(2), pp. 299–316.

[15] Suh, S. H., Woo, I. K., and Noh, S. K., 1991. "Development of an automatic trajectory planning system (atps) for spray painting robots". In Proceedings 1991 IEEE International Conference on Robotics and Automation, Vol. 3, pp. 1948–1955.

[16] Chen, H., Fuhlbrigge, T., and Li, X., 2008. "Automated industrial robot path planning for spray painting process: A review". In 2008 IEEE International Conference on Automation Science and Engineering, pp. 522–527.

[17] Kabir, A. M., Kaipa, K. N., Marvel, J., and Gupta, S. K., 2017. "Automated planning for robotic cleaning using multiple setups and oscillatory tool motions". *IEEE Transactions on Automation Science and Engineering,* ***14***(3), July, pp. 1364–1377.

[18] Kabir, A. M., Shah, B. C., and Gupta, S. K., 2018. "Trajectory planning for manipulators operating in confined workspaces". In 2018 IEEE International Conference on Automation Science and Engineering (CASE).

[19] Ding, D., Pan, Z., Cuiuri, D., Li, H., and Larkin, N., 2016. "Adaptive path planning for wire-feed additive manufacturing using medial axis transformation". *Journal of Cleaner Production,* ***133***, pp. 942–952.

[20] Zhang, G. Q., Mondesir, W., Martinez, C., Li, X., Fuhlbrigge, T. A., and Bheda, H., 2015. "Robotic additive manufacturing along curved surface - a step towards free-form fabrication". In 2015 IEEE International Conference on Robotics and Biomimetics (ROBIO), IEEE, pp. 721–726.

[21] Zhang, G. Q., Spaak, A., Martinez, C., Lasko, D. T., Zhang, B., and Fuhlbrigge, T. A., 2016. "Robotic additive manufacturing process simulation - towards design and analysis with building parameter in consideration". In 2016 IEEE International Conference on Automation Science and Engineering (CASE), pp. 609–613.

[22] Kucuk, S., and Bingul, Z., 2004. "The inverse kinematics solutions of industrial robot manipulators". In Mechatronics, 2004. ICM '04. Proceedings of the IEEE International Conference on, pp. 274–279.